Use of a PEG-conjugated bright near-infrared dye for functional imaging of rerouting of tumor lymphatic drainage after sentinel lymph node metastasis

Steven T. Proulx[1], **Paola Luciani**[1], **Ailsa Christiansen**[1], **Sinem Karaman**[1], **Katrin S. Blum**[1], **Matthias Rinderknecht**[1], **Jean-Christophe Leroux**[1], and **Michael Detmar**[1,*]

[1] Institute of Pharmaceutical Sciences, Swiss Federal Institute of Technology, ETH Zurich, 8093 Zurich, Switzerland

Abstract

Tumor lymphangiogenesis promotes metastatic cancer spread to lymph nodes and beyond. However, the potential remodeling and functionality of tumor-draining lymphatic vessels has remained unclear. Thus, we aimed to develop non-invasive imaging methods for repeated quantitative imaging of lymphatic drainage and of contractile collecting lymphatic vessel function in mice, with colloidal near-infrared (NIR) tracers and a custom fluorescence stereomicroscope specially adapted for NIR sensitive imaging. Using these tools, we quantitatively determined pulse rates and valvular function of collecting lymphatic vessels with high resolution. Unexpectedly, we found that tumor-draining lymphatic vessels in a melanoma footpad model initially were dilated but remained functional, despite lower pulse rates. In two independent tumor models, impaired lymphatic function was detected once metastases were present in draining lymph nodes. Importantly, we found that lymphatic dysfunction, induced by metastatic tumor spread to sentinel lymph nodes, can lead to a rerouting of lymphatic flow away from the metastatic lymph node, via collateral lymphatic vessels, to alternate lymph nodes. These findings might have important clinical implications for the procedure of sentinel lymph node mapping that represents the standard of care for determining prognosis and treatment of melanoma and breast cancer patients.

Keywords

lymph node; noninvasive imaging of animal models; lymphatic vessels; metastasis; polymers; liposomes

1. Introduction

The lymphatic system plays an important role in the maintenance of tissue fluid homeostasis, the initiation of immune responses and the uptake of dietary fats. Lymphatic vessels have received tremendous scientific interest recently since it was determined that

*Corresponding author: Michael Detmar, M.D. Institute of Pharmaceutical Sciences Swiss Federal Institute of Technology, ETH Zurich Wolfgang-Pauli-Str. 10, HCI H303 CH-8093 Zürich, Switzerland Tel.: ++41-44-633-7361 Fax: ++41-44-633-1364 michael.detmar@pharma.ethz.ch.

they also play key roles in pathological conditions such as chronic inflammation, transplant rejection, and tumor metastasis [1]. In particular, tumor-induced lymphangiogenesis in the peritumoral area and in tumor-draining lymph nodes (LN) has been found to promote metastatic cancer spread in several experimental models and clinical studies [2, 3]. Moreover, the presence of LN metastases represents a critical staging parameter to determine the prognosis and the course of therapy for the majority of cancer patients [4, 5]. Most studies thus far have focused on the molecular mechanisms that modulate tumor-induced initial lymphatic vessel growth but relatively little is known about the changes that take place in collecting lymphatic vessels. Unlike initial lymphatic vessels, collecting vessels have smooth muscle coverage and function through pulsatile contractions to transport lymphatic fluid through a system of one-way valves against an increasing hydrostatic pressure gradient [6, 7]. Despite the clinical importance of tumor lymphangiogenesis, controversy remains whether tumor-draining collecting lymphatic vessels remain functional and what changes are induced by the tumor-derived factors and by metastatic growth in the draining LNs [8-12].

One of the major reasons for the paucity of information on tumor-draining collecting lymphatic vessels are the technical obstacles associated with non-invasive quantitative functional lymphatic imaging. Studies on exteriorized mesentery have provided valuable insights into the physiology of collecting lymphatic vessels and the factors that control their contractile function [13]. More recently, an intravital microscopic approach for imaging popliteal collecting lymphatic vessels after FITC-dextran injection was described [14]. Although this technique allows excellent dynamic visualization, it also requires invasive surgery to exteriorize the vessels, which precludes any longitudinal imaging. Other currently used non-invasive techniques for lymphatic visualization, including lymphscintigraphy, positron emission tomography (PET), or magnetic resonance imaging (MRI) suffer from such limitations as poor spatial resolution, high costs for equipment and/or the need for radiotracers [15-18]. Moreover, the temporal resolution of these imaging modalities does not allow investigation of the pulsing dynamics of collecting lymphatic vessels.

Near-infrared (NIR) imaging has recently emerged as a promising tool to visualize lymphatic system in a non-invasive manner in both animal models and humans [10, 19-24]. The majority of previous studies have utilized either quantum dots (QD) or the NIR dye indocyanine green (ICG) as lymphatic tracers. Imaging with NIR QDs allows the visualization of sentinel nodes in mice and in large animals, however, phagocytosis of these nanocolloids and long-term retention in LNs limit their potential for longitudinal imaging and clinical translation [22, 23]. The advantages of ICG are that it has clinical approval with an excellent safety profile and that it binds serum proteins after tissue injection, facilitating its use as a lymphatic tracer [19]. However, ICG also has several non-optimal features. It is a dim dye and tends to aggregate in solution, leading to self-quenching effects. Additionally, there have been concerns of inhibition of lymphatic contractions due to the presence of ICG [25]. The limitations of existing tracers have led us to develop a research program to identify new macromolecular contrast agents for lymphatic imaging [10].

In the present study, we aimed to develop methods for quantitative, *in vivo* functional lymphatic imaging with high spatial and temporal resolution. To this end, we utilized poly(ethylene glycol) (PEG) conjugates of the bright NIR dye IRDye, and developed a NIR capable stereomicroscope to allow non-invasive visualization and quantification of the pulse rates and valvular function of collecting lymphatic vessels in mice. Using these tools, we assessed the function of tumor-draining collecting lymphatic vessels in two different tumor models and determined the changes in lymphatic drainage that take place before and after the development of lymph node metastases.

2. Materials and Methods

2.1 Mice

C57BL/6J-*Tyr*$^{c-2J}$/*J* albino (Jackson Laboratories, Bar Harbor, ME) and Balb/c (Janvier, Le Genest Saint Isle, France) mice were maintained in pathogen free conditions until imaging. Mice received an alfalfa-free diet (Experimental diet #2222, Provimi Kliba, Penthalaz, Switzerland) for at least four days prior to imaging. All animal experiments were approved by the Kantonales Veterinaeramt Zurich.

2.2 NIR lymphatic tracers

The PEG-based lymphatic tracers (Table 1) were prepared as described previously [26]. Shortly, 75 nmol of PEG amine P10 (10 kDa, NOF Europe, Grobbendonk, Belgium), P20 (20 kDa, Fluka, St. Louis, MO), or P40 (40 kDa, JenKem Technology USA Inc., Allen, TX), predissolved in dimethylsulphoxide, were reacted with an equimolar amount of IRDye® 800CW NHS Ester (D800, LI-COR Biosciences, Lincoln, NE) or IRDye® 680LT NHS Ester (D680, LI-COR Biosciences) at room temperature for 6 h. The crude reaction was lyophilized, reconstituted with 250 μL of HEPES buffered saline (HEPES 20 mmol/L, NaCl 142 mmol/L, pH 7.4), and purified twice by filtration using Fluorescent Dye Removal columns (Thermo Fisher Scientific, Rockford, IL). The efficiency of the coupling procedure was assessed spectrophotometrically and the purity of the final product verified via HPLC [26]. Concentration is expressed as μmol/L of dye content in the tracer.

The liposomal ICG (L-ICG), formulated with 1,2-dioleoyl-*sn*-glycero-3-phosphocholine (DOPC), cholesterol, and 1,2-distearoyl-*sn*-glycero-3-phosphoethanolamine-N-[methoxy(polyethylene glycol)-2000] (PEG-DSPE) (52.5:40:7.5 mol %, 7.8 mM total lipid concentration, 30 μM ICG), were prepared according to a previously published method (10). Their mean diameter was 66.8 ± 2.6 nm (*n*=6) and their polydispersity index was 0.105 ± 0.053, as measured by dynamic light scattering (DelsaNano Zetasizer, Beckmann-Coulter Inc., Fullerton, CA). The stability of the liposomes was checked over 42 days and no significant change in size was found. Freshly prepared L-ICG exhibited a 3-fold increase in fluorescence intensity with respect to free ICG, as well as an expected bathochromic shift in $\lambda_{max,em}$ (~17 nm).

2.3 NIR lymphatic imaging

A Zeiss StereoLumar.V12 (Carl Zeiss, Oberkochen, Germany) stereomicroscope with AxioVision (Zeiss) software was used for *in vivo* imaging of collecting lymphatic vessels. To allow far-red and NIR imaging, the following components were installed: a cooled EMCCD camera (Evolve eXcelon, Photometrics, Tuscon, AZ) with enhanced sensitivity to NIR wavelengths, a high-powered light emitting diode (LED) system with illumination at 470, 550, 635 and 770 nm (CoolLED, Andover, UK) and specific filters for FITC, Texas Red, Cy5 (Zeiss) and ICG (Semrock, Rochester, NY). Mice were anesthetized via intraperitoneal (i.p.) injection of 0.2 mg/kg medetomidine and 80 mg/kg ketamine. Care was taken to position the mice on a level imaging plane for improved visualization and to ensure that the collecting lymphatics were not pulsing against a gradient of gravity. For visualization and quantification of lower limb collecting lymphatic vessels, 5 μL of 25 μM P20D680 were injected intradermally into the dorsal skin of the rear paw. A sequence of 1 image/s at 100 ms exposure was acquired at 6x magnification of a region of interest containing collecting lymphatic vessels and the popliteal LN for a total of 5 min, with injection performed approximately 30 s into the video. A second video with the same acquisition settings was initiated with external compression performed 30 s into the video to enhance uptake of lymphatic tracer by the initial lymphatic vessels. Cyclic external compression was performed with a cotton swab lightly pressed on the intradermal injection

bleb once per second for 10 s. Additional higher zoom videos were acquired of collecting vessels at 15x and at the region of the popliteal LN at 12x (allowing visualization of afferent and efferent vessels). To test for flow impairment through draining LNs [10], imaging was performed after intradermal injection of L-ICG (5 μL of 30 μM ICG), as liposomes are confined to LN sinuses due to their size [27]. Imaging procedures to visualize other regions in the mouse are described in the individual figure legends.

2.4 Pulse rate analysis

Pulse rates were determined after injection of lymphatic tracers and after external compression of the injection site. Videos were analyzed in AxioVision software. During video playback, regions of interest were placed on popliteal afferent collecting vessels with care taken to avoid valve regions, typically seen as thicker knobs in the vessel morphology or at junctions with lymphatic tributaries. Each region of interest was evaluated for fluorescence intensity over time by using the Measure Profile function in Axiovision. Pulses were defined as one complete contraction (loss of fluorescent signal) and relaxation (gain of fluorescent signal) event and were counted starting from one minute after injection or external compression for three minutes.

2.5 Tumor models

B16.F10-luc2 murine melanoma cells (Caliper Life Sciences, Alameda, CA) were maintained in culture with DMEM medium (Invitrogen, Carlsbad, CA) containing 10% FBS. TdTomato fluorescent protein [28] was inserted into the pSNAP-tag (New England Biolabs, Ipswich, MA) vector and transfection of B16.F10-luc2 cells was performed by lipofectamine 2000 (Invitrogen). Stable clones (B16.F10-tdTom-luc2 cells) were selected by FACS sorting and maintained with addition of 1.6 mg/mL neomycin to the medium. B16.F10-tdTom-luc2 cells (2×10^5) in 10 μL PBS were injected into the right footpads of 9- to 11-week-old female C57BL/6J-Tyr^{c-J} albino mice. Tumors were allowed to grow for 33-35 days. An IVIS Spectrum (Xenogen, Caliper Life Sciences) was used for *in vivo* bioluminescence imaging of B16-F10-tdTom-luc2 LN metastases, as previously reported [10].

4T1 mammary carcinoma cells (ATCC) were maintained in DMEM medium (Invitrogen, Carlsbad, CA) containing 10% FBS. Cells were retrovirally transduced with MSCV-IRES-Venus (kind gift from Dr. Johannes Zuber, IMP, Vienna, Austria) using standard transduction techniques. Following transduction, FACS sorting was employed to obtain a stable population of 4T1-MSCV Venus cells with a high level of fluorescence. 4T1-MSCV-Venus cells (5×10^4) were injected subcutaneously into the rear right flank of 8-week old female Balb/c mice. Mice were imaged when tumors reached approximately 10 mm in diameter, typically 20-23 days after injection.

2.6 Statistical analyses

Data are represented as mean±SD. Data were analyzed using GraphPad Prism V5.0 (San Diego, CA) with the Student's *t*-test when comparisons were made between two groups and using ANOVA with Tukey's multiple comparison test when three of more groups were compared.

3. Results

3.1 Visualization of lymphatic vessels

To enable high resolution *in vivo* imaging of lymphatic vessels, we functionalized a Zeiss fluorescence stereomicroscope for NIR imaging by installation of a NIR sensitive camera and LED illumination system (Figure 1A). Video rate imaging was possible (up to 12

frames/s) with zoom factors ranging from 6x to 120x magnification. We first tested a range of different NIR tracers for potentially selective uptake by lymphatic vessels after intradermal injection (Table 1). We used a region of the lower leg that allowed visualization of collecting lymphatic vessels and of a large vein draining the intradermal injection site in the mouse paw. When unconjugated NIR dye IRDye 800CW (D800) was injected, venous uptake was clearly visible through the skin, along with limited perfusion of lymphatic vessels (Supplementary Figure S1A). The dye diffused quickly into the interstitium, consistent with previous data indicating that molecules less than 6 kDa easily diffuse out of collecting vessels [29]. When unconjugated ICG was injected, uptake was predominantly via lymphatic vessels (Supplementary Figure S1B) but ICG was clearly seen entering the blood vessels when the paw was manipulated to simulate movement (Video 1). Thus, commercial dyes revealed limited utility for the study of lymphatic vessels due to their small size [6]. Therefore, we tested PEG-based NIR tracers with larger molecular weight and size. Injection of the macromolecular conjugates P10D800 and P20D800 resulted in specific uptake only into lymphatic vessels (Supplementary Figures S1C and D), even after manipulation of the paw. Importantly, collecting vessel pulsations were clearly visualized (Video 1). Lymphatic specific uptake was also seen with the larger tracers P40D800 and L-ICG.

After intradermal injection of IRDye conjugates, initial and collecting lymphatic vessels could be non-invasively visualized at several anatomical locations with very low tissue autofluorescence with Cy5 or ICG filter sets. In the mouse tail, NIR imaging with P40D680 allowed visualization of two pulsing collecting vessels located under the skin on either side of the lateral tail vein (Figure 1B), in addition to the hexagonal dermal lymphatic pattern [30]. Lymphatic vessels of the ear (Figure 1C) and collecting lymphatic vessels of the flank (Figure 1D) could also be imaged with P20D800 and P40D680. However, the mouse limb was the most suitable site for visualization of a complete network of collecting vessels, including both the popliteal and the sciatic LNs (Figure 1E, Video 2). While either D680- and D800-based tracers resulted in excellent visualization of collecting lymphatic vessels at this region, D680 conjugates performed slightly better, likely due to increased dye quantum yield and brighter LED technology at this wavelength. We selected the P20D680 tracer for the development of longitudinal quantitative lymphatic imaging due to its smaller size (*vs.* P40D680), which facilitated interstitial diffusion and clearance from the injection site.

3.2 Quantification of pulse rates

We next investigated whether it was possible to noninvasively quantify the pulsatile function of collecting lymphatic vessels. We acquired videos of one acquisition per second of the lower limb of C57BL/6 albino mice during injection of P20D680 (Figure 2A). Shortly after injection, the popliteal afferent lymphatic vessels were perfused and pulsing was detected (Figure 2B, Video 3). After application of external compression to stimulate the initial lymphatic uptake of tracer, additional collecting vessels were perfused and pulse rates became more frequent and consistent between mice (12.7 ± 1.7 *vs.* 9.6 ± 2.6 pulses/min $p < 0.001$) (Figure 2C-E; Video 3). The entire collecting vessel network draining into the popliteal nodes, including both afferent lymphatic vessels, was consistently perfused, allowing pulse rate analyses to be performed non-invasively in multiple vessels simultaneously.

3.3 Visualization of tumor-draining lymphatic vessels

We next visualized the collecting lymphatic vessels that are draining from 4T1 murine breast tumors implanted subcutaneously in the rear flank. When tumors had reached approximately 10 mm in diameter, P40D800 tracer was injected peritumorally. Immediate uptake and transport of tracer by a tumor-draining collecting vessel into the large collecting

vessel on the flank that drains from the inguinal LN to the axillary LN was seen (Video 4). When collecting vessels were directly exposed, vessels draining tumors were dilated in comparison to non-tumor draining collecting vessels, but showed effective valve function without detectable backflow (Supplementary Figure S2 and Video 5). Thus, despite increased lymphatic flow from the tumor, collecting lymphatic vessels were able to adapt by increasing their diameter and by maintaining functionality of their one-way valves to prevent backflow.

We next investigated the lymphatic vessels draining B16 footpad melanomas over time (Figure 3A), in parallel to assessment of LN metastases by bioluminescence imaging at two different time points (days 18 and 32). A significant increase in bioluminescence of tumor-draining popliteal LNs was recorded on day 32 compared to day 18, with 3 of 6 animals demonstrating LN metastasis at this time (Figure 3B, Supplementary Figure S3). On the days following bioluminescence imaging (days 19 and 33), NIR imaging was performed with P20D680. Pulse rates in afferent lymphatic vessels were significantly decreased at day 19 (10.9±1.7 pulses/min, p<0.01) and day 33 (8.7±1.1 pulses/min, p<0.001) after tumor implantation, compared to baseline pulse rates before tumor implantation (13.0±0.81 pulses/min) (Figure 3C). However, no significant differences in pulse rates were found in efferent lymphatic vessels (Figure 3C). Closer examination revealed more dilated collecting vessels with irregular pulsing in mice that harbored LN metastases when compared to baseline or non-metastasis bearing mice (Figure 3D-G, Video 6). These data indicate that lymphatic drainage from the primary tumor remains functional but that metastatic growth in draining LNs might be correlated with impaired lymphatic function.

3.4 Impairment and rerouting of lymphatic drainage

The finding that mice with LN metastases appeared to have impaired lymphatic function, together with our previous finding of a negative correlation between lymphatic flow through LNs and the extent of metastases by B16 footpad melanomas [10], led us to investigate this phenomenon in further detail. We next imaged mice with confirmed LN metastases, using a B16-F10-luc2 cell line transfected with tdTomato fluorescent protein to enhance visualization of LN metastases by stereomicroscopy. At 35 days after implantation of tumor cells into the footpad, *in vivo* bioluminescence imaging was performed to confirm the presence of popliteal LN metastases. In these mice (*n*=8), we then performed stereomicroscope imaging of collecting lymphatic vessels. In mice harboring LN metastases, there was evidence of backflow through valves of collecting vessels that drained to sentinel LNs (Video 7). In one extreme case, there appeared to be a complete blockage of flow through the tumor-draining LN as assessed by L-ICG (Figure 4), which is confined to flow through LN sinuses due to its large size [27]. Five minutes after peritumoral injection of L-ICG, there were dramatic differences in the pulsing patterns of the two afferent vessels that were draining into the popliteal LN (Video 8 and Figure 4B). One vessel showed strong pulsations, while the other vessel showed only weak contractions. The LN showed increasing fluorescence signal intensity over time, indicating that the flow of L-ICG through the LN was impeded. Fluorescence imaging of the popliteal LN *in situ* revealed strong signal, originating from tdTomato expressing metastatic tumor cells, in one half of the node, near the point of entry of the dysfunctional afferent collecting vessel (Figure 4C-E).

Dysfunctional lymphatic flow might lead to interstitial accumulation of fluid, especially in tumors with increased vascular permeability. Consistent with this, mice with LN metastases had an increased interstitial diffusion of the lymphatic tracers in the peritumoral region, indicating that initial lymphatics had impaired lymphatic uptake (Figure 5A). Importantly, this interstitial spread of tracer led to the perfusion of pre-collector lymphatic vessels that were not draining to the larger collecting vessels leading to the popliteal LN. In total, 3 out of 8 mice examined with metastasis demonstrated a rerouting of flow away from the

lymphatic vessels that drained into the popliteal LN (Figure 5B and C and Video 9). These vessels instead drained towards the inguinal LN (Figure 5D), which contained tumor cells in two of the mice examined.

We next investigated in a second tumor model, the 4T1 breast tumor model, whether collecting lymphatic dysfunction might occur due to nodal metastatic growth. The 4T1 cells were retrovirally transduced with Venus fluorescent protein to allow the detection of metastases *in situ.* We then injected tumors subcutaneously into the flank of Balb/c mice. Notably, LN blockage by metastatic tumor cells was also found in this model, as peritumorally injected L-ICG was retained at the entrance of the afferent lymphatic vessel into the tumor-draining inguinal LN (Supplementary Figure S4A). Once this LN was exteriorized, a Venus[+] fluorescent signal, originating from metastatic tumor cells, was found in the region where the afferent vessel entered into the LN (Supplementary Figure S4B). Importantly, also in this model, a blockage of lymphatic flow to the sentinel node led to a rerouting pattern, with filling of the tracers into collateral vessels (Supplementary Figure S4C).

In summary, our results indicate that lymphatic flow can be obstructed by the growth of sentinel LN metastases. In some cases, this may result in rerouting of both lymphatic flow and the spread of tumor cells to alternative LNs (Figure 6).

4. Discussion

In this study, we have developed lymphatic-specific tracers and NIR imaging instrumentation for the non-invasive, quantitative *in vivo* imaging of lymphatic vessel drainage and contractile function. Despite the prevailing notion that free ICG binds albumin or other serum proteins after tissue injection and therefore might allow the specific imaging of lymphatic vessels, we found that a significant proportion of ICG enters into blood vessels, even at concentrations lower than those used in previous studies [20, 21]. These findings, together with its low quantum yield and the reported inhibition of lymphatic vessel pulsing [25], indicate that ICG is not the ideal tracer for quantitative NIR lymphatic imaging despite its current use in the clinic [24]. While L-ICG can increase brightness, stability and lymphatic specificity of ICG [10], concerns about its relatively large size and long term *in vivo* stability hinder its application to longitudinal quantitative lymphatic imaging. In contrast to ICG, our findings clearly reveal that PEG-IRDyes of molecular weight 10 kDa and above are exclusively drained by lymphatic vessels after tissue injection. Unlike previously employed lymphatic nanocolloids, the use of PEG-IRDye tracers prevented excessive phagocytosis and retention in draining LNs, issues that have hindered clinical translation of QDs [23]. We found that a tracer size of 20 kDa was ideal for efficient perfusion of collecting lymphatics and for enhanced interstitial diffusion and clearance from the injection site, enabling repeated, longitudinal imaging studies of the lymphatic system.

Using a specially NIR adapted stereomicroscope, these tracers enabled unprecedented quality of visualization of collecting lymphatic vessels and of draining LNs *in vivo.* NIR light allows deeper imaging through the skin resulting in an improved non-invasive visualization of lymphatic vessels, as compared to visible wavelengths. This was in particular revealed by the more detailed imaging of lymphatic vessels in the mouse tail compared with previous lymphangiography studies [30], and by the ability to visualize popliteal afferent lymphatic vessels without the need for surgical intervention [14]. Compared to previous NIR imaging approaches in mice, which typically use a whole-animal macroscopic imaging approach [10, 20], the imaging methods developed here demonstrated significant improvements in both spatial and temporal resolution. Video rate imaging at the

level of a single collecting lymphatic vessel was achieved allowing for visualization of pulsatile dynamics and valvular function.

Quantitative assessments of flow and pulsatile function in collecting lymphatic vessels are challenging due to the wide range of extrinsic and intrinsic factors that affect the contractility of these vessels [6, 7, 31]. It is generally accepted that extrinsic factors play the major role by generating periodic interstitial pressure fluctuations that open and close the overlapping junctions between endothelial cells, allowing the entry of fluid [32, 33]. These extrinsic factors include skeletal muscle movement, breathing, and arteriole pulse and vasomotion [7, 31]. In contrast, intrinsic contractility is critical for the transport of lymph in collecting vessels. Acute increases in fluid load cause vessel distension to trigger the contractions of these vessels [34], and many other factors affect their intrinsic contractility [13]. Studies of lymphatic function are further complicated by the fact that a subject at rest under anesthesia has a greatly diminished uptake of tracers into the initial lymphatics [7, 31]. Perhaps due to these challenges, there has been controversy whether peripheral collecting lymphatic vessels in mice pulse or not [35], even though intrinsic contractility of murine lymphatics was demonstrated as early as 1949 [36]. Since imaging in mice is not possible without anesthesia, we assessed pulse rates after external compression of the injection site to stimulate lymphatic uptake. This led to consistent perfusion and pulse rates that are in agreement with previous findings in mesenteric vessels in mice and in isolated rat mesenteric vessels [35, 37].

Our findings of functional flow in tumor-draining collecting lymphatic vessels before the development of LN metastases are in contrast to previous concepts of impaired lymphatic function associated with tumor growth [38] but are in line with recent reports of increased flow through LNs in experimental tumor models [9, 10]. The decreases in lymphatic vessel pulse rate with tumor progression appeared at first surprising, given the increased intralymphatic pressure due to the increased fluid load from the tumor. However, there is evidence that vessel dilation might correlate with dysfunction. Dilated vessels are associated with slower pulse rates and/or with a reduced ability of valves to close, indicating a limited ability of the distended vessel to contract [21, 39, 40]. Chronic exposure to factors draining from the tumor, such as nitric oxide or inflammatory mediators, might also have direct effects on the dilation and contractility of collecting lymphatic vessels [14, 41]. Indeed, addition of supernatant from a B16 melanoma cell line to isolated murine collecting lymphatic vessels resulted in a 40% inhibition of pulsing frequencies [42], similar to the 33% reduction in pulse rates that we determined *in vivo* from baseline to day 33 of tumor growth. Further studies are needed to investigate which tumor derived factors may influence collecting lymphatic vessel function.

Despite decreased pulse rates, there was sufficient lymphatic transport from the tumors until downstream obstructions were present. Resistance to flow in metastatic LNs may be as important to lymphatic dysfunction as the tumor effects on the lymphatic vessels themselves, since we previously found that flow through tumor-draining LNs was inversely correlated to the bioluminescence signal created by LN metastases [10]. This is in agreement with reported changes in lymphatic flow once metastases are present [12, 43] and similar to other cases where LN flow resistance was experimentally induced [44, 45]. Interestingly, unlike afferent vessels, we found no differences in efferent popliteal lymphatic vessel pulse rates during the progression of the tumor, perhaps indicating that the LN is able to "normalize" dysfunction to some degree by either fluid exchange mechanisms or by venous absorption of contractility inhibitors [46]. Whether this preservation of efferent lymphatic function could possibly contribute to the further spread of tumor cells from LN metastases remains to be determined.

Importantly, our study demonstrated a rerouting of tumor drainage after the establishment of sentinel LN metastasis. This rerouting might have been due to *de novo* growth of lymphatic vessels or by allowing access to preexisting collateral lymphatic vessels. Although it is widely accepted that tumor-associated initial lymphatic vessels and lymphatic sinuses in LNs remodel [1, 3], remodeling and formation of new tumor-draining collecting lymphatic vessels has not been reported. We found increased interstitial diffusion of the injected tracers from the tumors towards functional collecting vessels, supporting a hypothesis of rerouting of fluid towards a "path of least resistance" into preexisting vessels.

5. Conclusions

Our results reveal for the first time in an experimental setting that the growth of metastases can lead to lymphatic flow obstructions in the primary draining LN, which may result in rerouting of lymph flow - and potentially cancer spread - to alternate LNs. This concept might have major clinical relevance for the procedure of sentinel LN mapping and dissection, which is currently the standard of care in melanoma and breast cancer [4]. Metastatic sentinel LNs might not be detected due to lymphatic vessel obstruction and rerouting of the drainage of peritumorally injected tracer to different LNs. Our findings provide a functional explanation for the clinically reported findings of lymphatic obstruction in melanoma, penile cancer and breast cancer patients [47-49] that could result in a higher rate of false negatives during LN mapping procedures. The fact that NIR technology is already established and clinically used should facilitate the translation of more sophisticated *in vivo* imaging techniques that can help to detect LN metastases even in the presence of obstructed lymphatic transport.

Supplementary Material

Refer to Web version on PubMed Central for supplementary material.

Acknowledgments

References

1. Alitalo K. The lymphatic vasculature in disease. Nat Med. 2011; 17:1371–80. [PubMed: 22064427]

2. Van den Eynden GG, Vandenberghe MK, van Dam PJ, Colpaert CG, van Dam P, Dirix LY, et al. Increased sentinel lymph node lymphangiogenesis is associated with nonsentinel axillary lymph node involvement in breast cancer patients with a positive sentinel node. Clin Cancer Res. 2007; 13:5391–7. [PubMed: 17875768]

3. Mumprecht V, Detmar M. Lymphangiogenesis and cancer metastasis. J Cell Mol Med. 2009; 13:1405–16. [PubMed: 19583813]

4. Giuliano AE, Kirgan DM, Guenther JM, Morton DL. Lymphatic mapping and sentinel lymphadenectomy for breast cancer. Ann Surg. 1994; 220:391–8. discussion 8-401. [PubMed: 8092905]

5. Sleeman JP, Nazarenko I, Thiele W. Do all roads lead to Rome? Routes to metastasis development. Int J Cancer. 2011; 128:2511–26. [PubMed: 21365648]

6. Swartz MA. The physiology of the lymphatic system. Adv Drug Deliv Rev. 2001; 50:3–20. [PubMed: 11489331]

7. Schmid-Schonbein GW. Microlymphatics and lymph flow. Physiol Rev. 1990; 70:987–1028. [PubMed: 2217560]

8. Padera TP, Kadambi A, di Tomaso E, Carreira CM, Brown EB, Boucher Y, et al. Lymphatic metastasis in the absence of functional intratumor lymphatics. Science. 2002; 296:1883–6. [PubMed: 11976409]

9. Harrell MI, Iritani BM, Ruddell A. Tumor-induced sentinel lymph node lymphangiogenesis and increased lymph flow precede melanoma metastasis. Am J Pathol. 2007; 170:774–86. [PubMed: 17255343]

10. Proulx ST, Luciani P, Derzsi S, Rinderknecht M, Mumprecht V, Leroux JC, et al. Quantitative imaging of lymphatic function with liposomal indocyanine green. Cancer Res. 2010; 70:7053–62. [PubMed: 20823159]

11. Hoshida T, Isaka N, Hagendoorn J, di Tomaso E, Chen YL, Pytowski B, et al. Imaging steps of lymphatic metastasis reveals that vascular endothelial growth factor-C increases metastasis by increasing delivery of cancer cells to lymph nodes: therapeutic implications. Cancer Res. 2006; 66:8065–75. [PubMed: 16912183]

12. Dadiani M, Kalchenko V, Yosepovich A, Margalit R, Hassid Y, Degani H, et al. Real-time imaging of lymphogenic metastasis in orthotopic human breast cancer. Cancer Res. 2006; 66:8037–41. [PubMed: 16912179]

13. Zawieja DC. Contractile physiology of lymphatics. Lymphat Res Biol. 2009; 7:87–96. [PubMed: 19534632]

14. Liao S, Cheng G, Conner DA, Huang Y, Kucherlapati RS, Munn LL, et al. Impaired lymphatic contraction associated with immunosuppression. Proc Natl Acad Sci U S A. 2011; 108:18784–9. [PubMed: 22065738]

15. Zhang F, Niu G, Lu G, Chen X. Preclinical lymphatic imaging. Mol Imaging Biol. 2011; 13:599–612. [PubMed: 20862613]

16. Mumprecht V, Honer M, Vigl B, Proulx ST, Trachsel E, Kaspar M, et al. In vivo imaging of inflammation- and tumor-induced lymph node lymphangiogenesis by immuno-positron emission tomography. Cancer Res. 2010; 70:8842–51. [PubMed: 20978206]

17. Proulx ST, Kwok E, You Z, Beck CA, Shealy DJ, Ritchlin CT, et al. MRI and quantification of draining lymph node function in inflammatory arthritis. Ann N Y Acad Sci. 2007; 1117:106–23. [PubMed: 17646265]

18. Ruddell A, Harrell MI, Minoshima S, Maravilla KR, Iritani BM, White SW, et al. Dynamic contrast-enhanced magnetic resonance imaging of tumor-induced lymph flow. Neoplasia. 2008; 10:706–13. [PubMed: 18592009]

19. Sharma R, Wendt JA, Rasmussen JC, Adams KE, Marshall MV, Sevick-Muraca EM. New horizons for imaging lymphatic function. Ann N Y Acad Sci. 2008; 1131:13–36. [PubMed: 18519956]

20. Kwon S, Sevick-Muraca EM. Functional lymphatic imaging in tumor-bearing mice. J Immunol Methods. 2010; 360:167–72. [PubMed: 20600076]

21. Zhou Q, Wood R, Schwarz EM, Wang YJ, Xing L. Near-infrared lymphatic imaging demonstrates the dynamics of lymph flow and lymphangiogenesis during the acute versus chronic phases of arthritis in mice. Arthritis Rheum. 2010; 62:1881–9. [PubMed: 20309866]

22. Kim S, Lim YT, Soltesz EG, De Grand AM, Lee J, Nakayama A, et al. Near-infrared fluorescent type II quantum dots for sentinel lymph node mapping. Nat Biotechnol. 2004; 22:93–7. [PubMed: 14661026]

23. Kosaka N, Ogawa M, Sato N, Choyke PL, Kobayashi H. In vivo real-time, multicolor, quantum dot lymphatic imaging. J Invest Dermatol. 2009; 129:2818–22. [PubMed: 19536144]

24. Rasmussen JC, Tan IC, Marshall MV, Fife CE, Sevick-Muraca EM. Lymphatic imaging in humans with near-infrared fluorescence. Curr Opin Biotechnol. 2009; 20:74–82. [PubMed: 19233639]

25. Gashev AA, Nagai T, Bridenbaugh EA. Indocyanine green and lymphatic imaging: current problems. Lymphat Res Biol. 2010; 8:127–30. [PubMed: 20583875]

26. Proulx ST, Luciani P, Alitalo A, Mumprecht V, Christiansen AJ, Huggenberger R, et al. Non-invasive dynamic near-infrared imaging and quantification of vascular leakage in vivo. Angiogenesis. 2013 DOI: 10.1007/s10456-013-9332-2.

27. Gretz JE, Norbury CC, Anderson AO, Proudfoot AE, Shaw S. Lymph-borne chemokines and other low molecular weight molecules reach high endothelial venules via specialized conduits while a functional barrier limits access to the lymphocyte microenvironments in lymph node cortex. J Exp Med. 2000; 192:1425–40. [PubMed: 11085745]

28. Trichas G, Begbie J, Srinivas S. Use of the viral 2A peptide for bicistronic expression in transgenic mice. BMC Biol. 2008; 6:40. [PubMed: 18793381]

29. Mayerson, H. The physiologic importance of lymph.. In: Hamilton, W., editor. Circulation. American Physiological Society; Washington, DC: 1963. p. 1035-73.

30. Leu AJ, Berk DA, Yuan F, Jain RK. Flow velocity in the superficial lymphatic network of the mouse tail. Am J Physiol. 1994; 267:H1507–13. [PubMed: 7943396]

31. Aukland K, Reed RK. Interstitial-lymphatic mechanisms in the control of extracellular fluid volume. Physiol Rev. 1993; 73:1–78. [PubMed: 8419962]

32. Schmid-Schonbein GW. The second valve system in lymphatics. Lymphat Res Biol. 2003; 1:25–9. discussion 9-31. [PubMed: 15624318]

33. Baluk P, Fuxe J, Hashizume H, Romano T, Lashnits E, Butz S, et al. Functionally specialized junctions between endothelial cells of lymphatic vessels. J Exp Med. 2007; 204:2349–62. [PubMed: 17846148]

34. McHale NG, Roddie IC. The effect of transmural pressure on pumping activity in isolated bovine lymphatic vessels. J Physiol. 1976; 261:255–69. [PubMed: 988184]

35. Gashev AA, Davis MJ, Gasheva OY, Nepiushchikh ZV, Wang W, Dougherty P, et al. Methods for lymphatic vessel culture and gene transfection. Microcirculation. 2009; 16:615–28. [PubMed: 19626551]

36. Smith RO. Lymphatic contractility; a possible intrinsic mechanism of lymphatic vessels for the transport of lymph. J Exp Med. 1949; 90:497–509. [PubMed: 18143591]

37. Ono N, Mizuno R, Nojiri H, Ohhashi T. Development of an experimental apparatus for investigating lymphatic pumping activity of murine mesentery in vivo. Jpn J Physiol. 2000; 50:25–31. [PubMed: 10866694]

38. Isaka N, Padera TP, Hagendoorn J, Fukumura D, Jain RK. Peritumor lymphatics induced by vascular endothelial growth factor-C exhibit abnormal function. Cancer Res. 2004; 64:4400–4. [PubMed: 15231646]

39. Wu TF, Carati CJ, Macnaughton WK, von der Weid PY. Contractile activity of lymphatic vessels is altered in the TNBS model of guinea pig ileitis. Am J Physiol Gastrointest Liver Physiol. 2006; 291:G566–74. [PubMed: 16675748]

40. Davis MJ, Rahbar E, Gashev AA, Zawieja DC, Moore JE Jr. Determinants of valve gating in collecting lymphatic vessels from rat mesentery. Am J Physiol Heart Circ Physiol. 2011; 301:H48–60. [PubMed: 21460194]

41. Von Der Weid PY, Rehal S. Lymphatic pump function in the inflamed gut. Ann N Y Acad Sci. 2010; 1207(Suppl 1):E69–74. [PubMed: 20961308]

42. Nakaya K, Mizuno R, Ohhashi T. B16-BL6 melanoma cells release inhibitory factor(s) of active pump activity in isolated lymph vessels. Am J Physiol Cell Physiol. 2001; 281:C1812–8. [PubMed: 11698239]

43. Van De Velde CJ, Van Putten LM, Zwaveling A. A new metastasizing mammary carcinoma model in mice: model characteristics and applications. Eur J Cancer. 1977; 13:555–65. [PubMed: 880963]

44. Browse NL, Doig RL, Sizeland D. The resistance of a lymph node to lymph flow. Br J Surg. 1984; 71:192–6. [PubMed: 6697120]

45. Nagai T, Ikomi F, Suzuki S, Ohhashi T. In situ lymph dynamic characterization through lymph nodes in rabbit hind leg: special reference to nodal inflammation. J Physiol Sci. 2008; 58:123–32. [PubMed: 18325146]

46. Adair TH, Moffatt DS, Paulsen AW, Guyton AC. Quantitation of changes in lymph protein concentration during lymph node transit. Am J Physiol. 1982; 243:H351–9. [PubMed: 7114267]

47. Lam TK, Uren RF, Scolyer RA, Quinn MJ, Shannon KF, Thompson JF. False-negative sentinel node biopsy because of obstruction of lymphatics by metastatic melanoma: the value of ultrasound

in conjunction with preoperative lymphoscintigraphy. Melanoma Res. 2009; 19:94–9. [PubMed: 19262412]

48. Leijte JA, van der Ploeg IM, Valdes Olmos RA, Nieweg OE, Horenblas S. Visualization of tumor blockage and rerouting of lymphatic drainage in penile cancer patients by use of SPECT/CT. J Nucl Med. 2009; 50:364–7. [PubMed: 19223404]

49. Nathanson SD, Mahan M. Sentinel lymph node pressure in breast cancer. Ann Surg Oncol. 2011; 18:3791–6. [PubMed: 21626079]
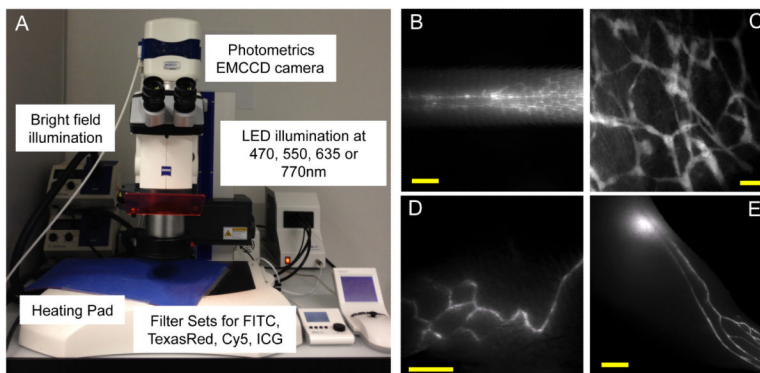
Figure 1.
NIR fluorescence stereomicroscope instrumentation and visualization of lymphatic vessels with lymphatic tracers in C57BL/6 albino mice. **(A)** Stereomicroscope setup for *in vivo* imaging with four separate LED illumination wavelengths and NIR sensitive EMCCD camera. **(B)** Imaging of lateral side of the tail after intradermal injection of 3 µL of 25 µM P40D680 with visualization of superficial lymphatics and two deeper collecting vessels. Scale bar: 2 mm. **(C)** Imaging of ear lymphatic vessels after intradermal injection of 1 µL of 50 µM P20D800 into ear tip. Scale bar: 200 µm. **(D)** Visualization of collecting vessels of the flank after intradermal injection of 10 µL of 25 µM P40D680 at the tail base. Scale bar: 2 mm. **(E)** Imaging of collecting vessels in the lower leg and popliteal LN after intradermal injection of 5 µL of 25 µM P20D680 into foot skin. Scale bar: 2 mm.
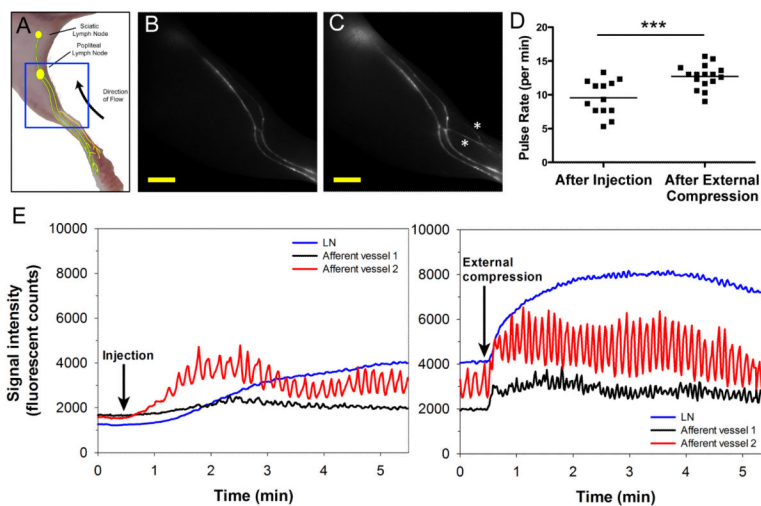
Figure 2.
Effect of external compression on lymphatic vessel perfusion and collecting vessel pulse rates in C57BL/6 albino mice (n=8). **(A)** Cartoon of lymphatic vessel network draining the hind limb of a mouse with blue box indicating imaged region. **(B)** Representative video frame after intradermal injection of 5 µL of 25 µM P20D680 into hind paw showing uptake into collecting vessels. Scale bar: 2 mm. **(C)** Same mouse after external compression, showing higher fluorescence intensity in afferent vessels and draining LN. Additional perfused lymphatic vessels are indicated with white asterisks. Scale bar: 2 mm. **(D)** Pulse rate analysis of afferent collecting vessels (n=2 per mouse), performed for 3 min starting one minute after injection or compression. Three afferent vessels were insufficiently perfused to perform analysis after injection. ***p<0.001. **(E)** Representative plots showing fluorescent signals in afferent vessels and popliteal LN in a representative mouse after injection (left) and external compression (right). Sustained increases in pulse rates are seen in both afferent vessels with higher fluorescent intensity, indicating increased perfusion of the vessels and LN.
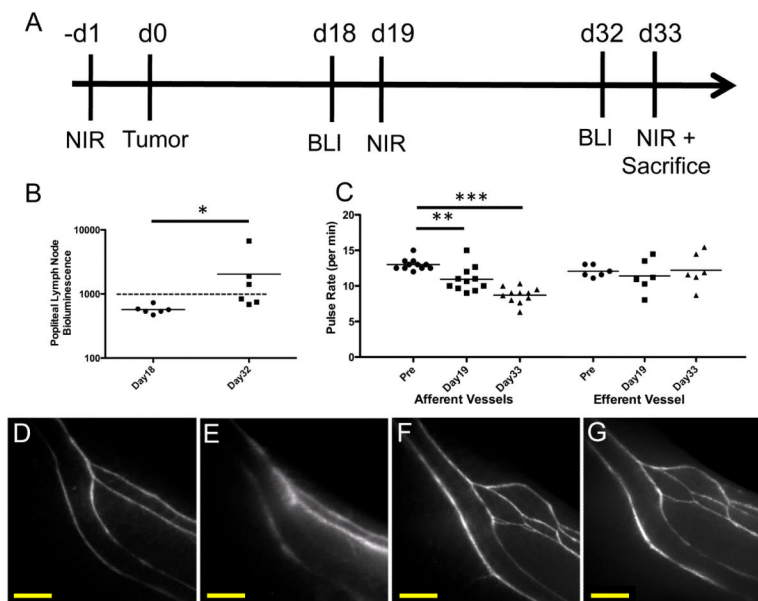
Figure 3.
Longitudinal pulse rate analysis of collecting lymphatic vessels with P20D680 and LN metastasis detection after B16 footpad tumor induction (n=6). **(A)** Timeline of tumor induction (at day 0) and longitudinal imaging timepoints (BLI: bioluminescent imaging, NIR: Near-infrared collecting vessel analysis). **(B)** Quantification of *in vivo* bioluminescence imaging of popliteal LN for detection of metastases at days 18 and 32 after tumor induction. Bioluminescent signal is shown in photons/s/cm^2/sr. Dashed line indicates threshold for LN positive for metastasis. * indicates p<0.05. **(C)** Quantification of pulse rates of afferent (n=2 per mouse) and efferent popliteal collecting lymphatics before and at days 19 and 33. **p<0.01, ***p<0.001. **(D)** Representative image of collecting lymphatic vessels in lower limb before tumor induction. **(E)** Image of collecting vessels in the same mouse at day 33 after bioluminescent tumor signal was found in the popliteal LN. **(F and G)** Representative images of collecting vessels in a different mouse before and at day 33 with no metastatic LN signals. Scale bars: 1 mm.
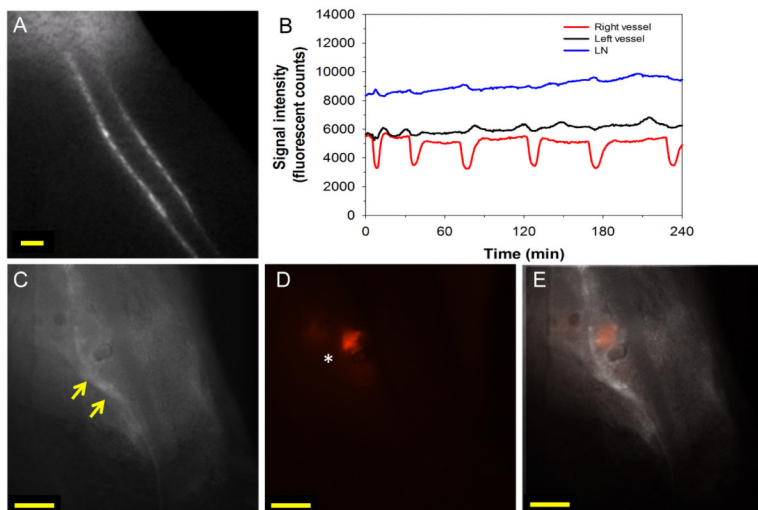
Figure 4.
Dysfunction of popliteal collecting lymphatic vessels in a B16 footpad tumor bearing mouse with LN metastases. **(A)** Screen capture of video beginning five minutes after L-ICG injection (5 µL of 30 µM) into hind paw. **(B)** Quantification of afferent popliteal collecting lymphatic pulsing and LN fluorescent signal demonstrating strong pulses in right afferent vessel with irregular pulses in left afferent vessel. **(C)** NIR image of popliteal LN after skin removal showing intense L-ICG signal at junction of left afferent vessel and LN (yellow arrows). **(D)** Fluorescent image demonstrating strong tdTomato signal on left side of popliteal LN (white asterisk). **(E)** Overlay of images demonstrating strong tdTomato signal in LN at site of afferent vessel entry into popliteal LN. Scale bars: 500 µm.
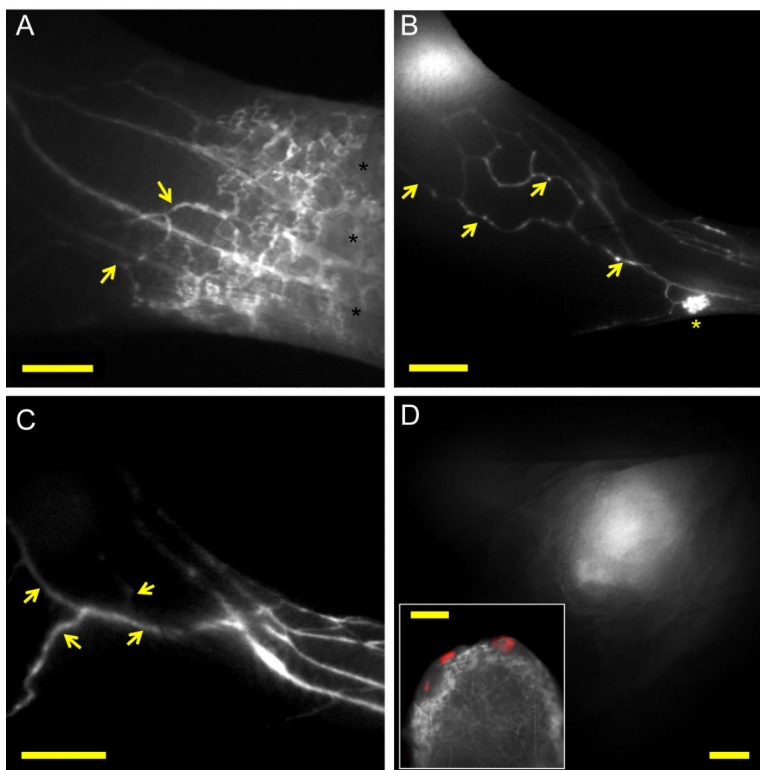
Figure 5.
Lymphatic dysfunction and rerouting of lymphatic flow in mice bearing B16 footpad tumors with popliteal LN metastases. **(A)** Imaging of dermal and collecting lymphatic vessels in the lower limb after P40D680 injection, demonstrating increased interstitial signal in the dermal region (black asterisks) and uptake by collateral vessels (yellow arrows). Scale bar: 1 mm. **(B)** Representative image after P40D680 injection of a mouse with rerouted flow toward collecting vessel network (yellow arrows) that drains towards the inguinal LN. Dermal backflow is seen in one region of the skin (yellow asterisk) Scale bar: 2 mm. **(C)** Representative image after ICG liposome injection of a mouse with more extensive rerouting of flow into dilated collateral vessels (yellow arrows) that drain towards the inguinal LN. Scale bar: 2 mm. **(D)** NIR image of the inguinal LN of the mouse shown in (C) demonstrating intense ICG liposome signal. Scale bar: 1 mm. Inset shows merged *ex vivo* image of tdTomato positive cells (red) in the inguinal node with no colocalization with ICG liposome signal in lymphatic sinus. Inset scale bar: 500 μm.
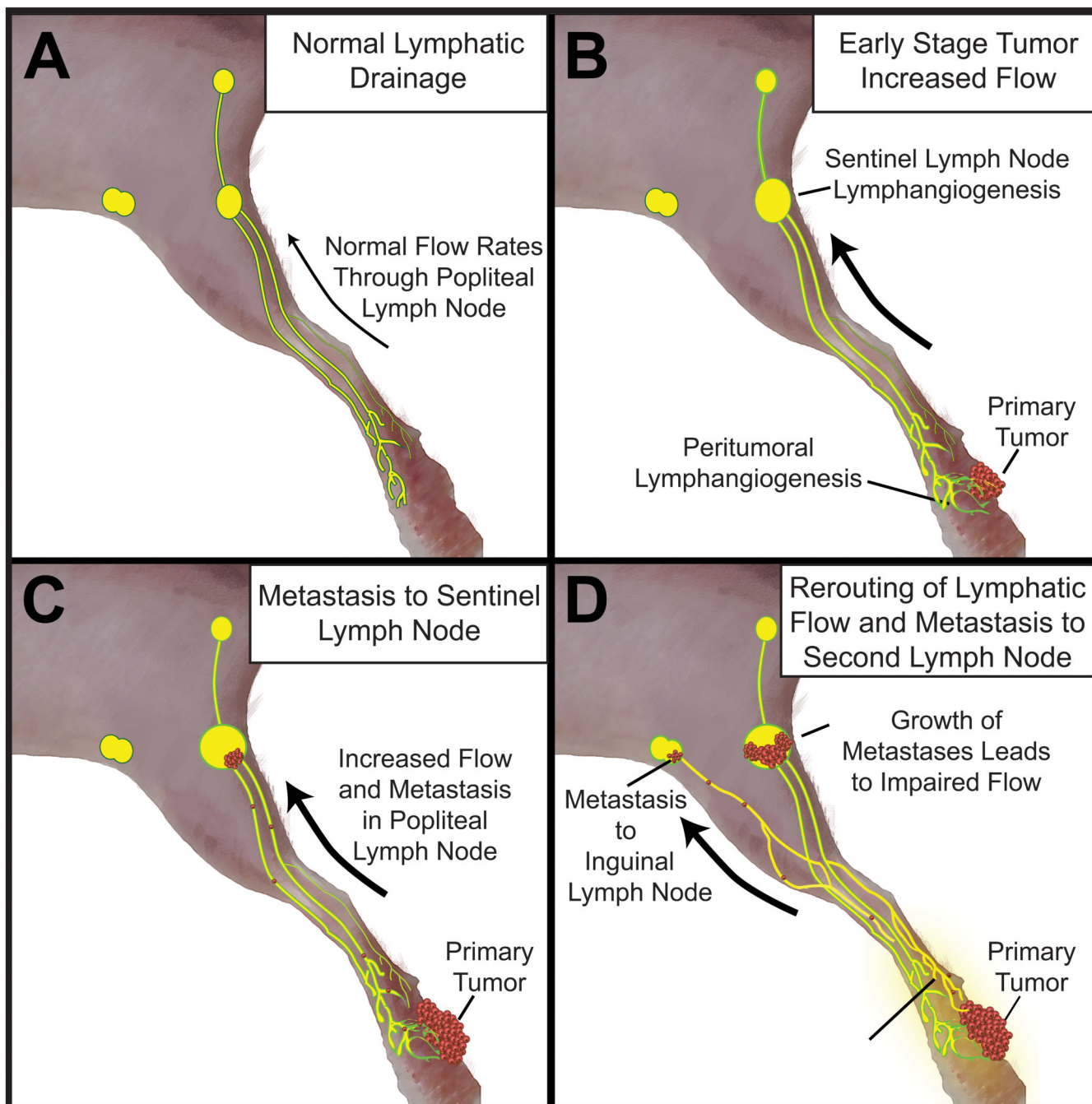
Figure 6.
Model of lymphatic flow and tumor spread from footpad tumors. **(A)** Normal drainage pattern from footpad through two afferent vessels through popliteal LN to efferent lymphatic draining into sciatic LN. **(B)** After tumor induction and early stage growth, expansion of lymphatic network though lymphangiogenesis leads to increased flow from tumor. **(C)** Increased lymphatic flow and seeding of metastases to popliteal LN. **(D)** Growth of metastases in popliteal LN may induce lymphatic dysfunction and impaired flow through this route, which leads to a rerouting of flow towards alternate LNs. Eventually, metastasis may occur in the alternate inguinal LN.

Table 1

NIR tracers for lymphatic imaging of collecting vessels. The performance of each tracer was tested after intradermal injection into the paw, and videos were acquired of a region comprising of blood and lymphatic vessels draining the injection site (Supplementary Figure 1 and Movie S1). The diameters (given range between minimal and maximal projection) of D800 and ICG were computed from the molecular geometry of the lower energy conformers by using Marvin Calculator Plugins version 5.10.3, 2012, ChemAxon (http://www.chemaxon.com). The hydrodynamic radius of P10, P20, P40 were calculated as described in [26]. The hydrodynamic diameter of L-ICG was measured by dynamic light scattering as described in Materials and Methods.

NIR Tracer	Abbreviation	Excitation / Emission wavelength (nm)	Diameter (nm)	Blood uptake	Lymphatic uptake	Comments
IRDye800 CW	D800	778 / 794	2.2 - 2.6	+++	+	Leaks from collecting lymphatic vessels
Indocyanine green dye	ICG	785 / 815	1.7 - 2.6	+	++	Final size and lymphatic specificity dependent on protein binding
IRDye-PEG 10 kDa	P10D680 or P10D800	676/693 or 778 / 794	6.2	0	++	Easily diffuses through interstitium making it more difficult to perfuse collecting lymphatic vessels
IRDye-PEG 20 kDa	P20D680 or P20D800	676/693 or 778 / 794	8.4	0	+++	Small size enhances clearance from the injection site for longitudinal imaging
IRDye-PEG 40 kDa	P40D680 or P40D800	676/693 or 778 / 794	11.6	0	+++	Excellent perfusion of lymphatic vessels but slow clearance from injection site
ICG liposomes	L-ICG	720 / 832	67	0	+++	Excellent perfusion of lymphatic vessels, confined to sinuses in LN